Density Functional Theory Studies of Spin, Charge, and Orbital Ordering in YBaT$_2$O$_5$ (T = Mn, Fe, Co)

R. Vidya,[*,†] P. Ravindran,[†] K. Knizek,[‡] A. Kjekshus,[†] and H. Fjellvåg[†]

Center for Materials Science and Nanotechnology, Department of Chemistry, University of Oslo, Box 1033 Blindern, N-0315 Oslo, Norway, and Institute of Physics ASCR, Cukrovanicka 10, 162 53 Prague, Czech Republic

Spin, charge, and orbital orderings are influenced by electron/hole doping, cation radii, oxygen stoichiometry, temperature, magnetic field, and so on. In order to understand the role of electron/hole doping, we have studied variations in spin, charge, and orbital ordering in terms of d-band filling for YBaT$_2$O$_5$ (T = Mn, Fe, Co). The calculations were performed using density functional theory as implemented in the full-potential linearized augmented-plane-wave method. We have carried out calculations for nonmagnetic, ferromagnetic, and antiferromagnetic configurations. A ferrimagnetic ground state was established for YBaMn$_2$O$_5$, whereas YBaFe$_2$O$_5$ and YBaCo$_2$O$_5$ have antiferromagnetic ground states; all of these results are in agreement with experimental findings. The effects of spin−orbit coupling, the Hubbard *U* parameter, and orbital polarization on the magnetic properties were also analyzed. The electronic band characteristics were analyzed using total as well as site- and orbital-projected densities of states. Inclusion of spin−orbit coupling and Coulomb correlation effects in the calculations was found to be important in order to reproduce the experimentally established semiconducting behaviors of YBaFe$_2$O$_5$ and YBaCo$_2$O$_5$. In order to quantify the charges at each atomic site, we made use of the Bader "atom-in-molecule" concept and Born effective-charge (BEC) analyses. The structural optimizations and BEC tensor calculations were performed using the VASP-PAW method. The different types of charge and orbital orderings in these compounds were visualized using the energy-projected density matrices of the d electrons. Substantial differences in ordering patterns with respect to d-band filling emerged. Ordering of the d$_{z^2}$ orbital of Mn in YBaMn$_2$O$_5$ gave rise to *G*-type ferrimagnetic spin ordering along the *c* direction and checkerboard-type charge ordering, whereas ordering of the d$_{x^2-y^2}$ orbital of Fe in YBaFe$_2$O$_5$ caused Wollan−Koehler *G*-type antiferromagnetic spin ordering along the *b* direction and stripe-type charge ordering. Similarly, a complex pattern of orbital ordering in YBaCo$_2$O$_5$ activated spin and charge orderings similar to those in YBaFe$_2$O$_5$.

I. Introduction

The concept of colossal magnetoresistance (CMR) has received immense attention in recent years. CMR materials display a fascinating diversity in behaviors, including several forms of spin, charge, and orbital ordering (abbreviated as SO, CO, and OO, respectively).[1] A great deal of experimental and theoretical effort has been devoted to the study of manganites. The complexity of the manganites not only makes understanding these compounds very difficult but also brings out a wealth of fascinating physics. Therefore, this research has expanded toward other transition-metal oxides, as they may reveal clues to the behavior of manganites and exhibit some interesting phenomena themselves. In fact, such efforts have resulted in fruitful discoveries such as charge and spin ordering in analogous oxides of iron, cobalt, and nickel.[2–4] The electrical and magnetic properties related to

* To whom correspondence should be addressed. E-mail: vidya.ravindran@kjemi.uio.no.
† University of Oslo.
‡ Institute of Physics ASCR.

(1) Millis, A. J. In *Colossal Magnetoresistance Oxides*; Tokura, Y. Ed.; Gordon and Breach: Amsterdam, 2000; p 53.

(2) Woodward, P. M.; Karen, P. *Inorg. Chem.* **2003**, *42*, 1121.
(3) Vogt, T.; Woodward, P. M.; Karen, P.; Hunter, B. A.; Henning, P.; Moodenbaugh, A. R. *Phys. Rev. Lett.* **2000**, *84*, 2969.
(4) Tranquada, J. M.; Buttrey, D. J.; Sachan, V.; Lorenzo, J. E. *Phys. Rev. Lett.* **1994**, *73*, 1003.

CMR behavior are largely determined by the chemical composition and crystal structure of the given material, and such properties are often quite sensitive to even tiny changes.[5–10]

The coordination polyhedra around transition-metal (T) ions in oxides are sometimes distorted (e.g., by elongation of certain interatomic distances relative to others), thereby converting energy-degenerate d levels of the central T atom into nondegenerate levels. Such a process, known as Jahn−Teller distortion (JTD),[11] lowers the symmetry and decreases the total energy of the system. As a result of such distortion, the electrons are often localized at particular atomic sites, resulting in CO. In other words, preferential occupation of the d orbitals (normally resulting in OO) is believed to be one of the driving forces for JTD and the associated CO. SO is intimately connected with JTD, and CO transitions are accordingly expected to be coupled with OO and SO transitions.

In order to understand the role of cation radii and oxygen stoichiometry, we have previously reported detailed analyses of SO, CO, and OO in YBaMn$_2$O$_5$ (YBMO5)[12,13] and LaBaMn$_2$O$_{5+\delta}$ ($0 \leq \delta \leq 1$).[14] On the basis of the rigid-band approximation, progressive filling of d orbitals should shift the Fermi level (E_F) toward the conduction band and therefore play an important role in spin and orbital dynamics. Hence, in this work we have concentrated our efforts on elucidating the effects of d-orbital filling on SO, CO, and OO in YBMO5, YBaFe$_2$O$_5$ (YBFO5), and YBaCo$_2$O$_5$ (YBCO5).

The chemical and crystallographic compositions of the YBaT$_2$O$_5$ phases are interesting because the presence of equal numbers of charged T atoms in two different valence (charge) states should maximize the Coulomb stabilization energy of a CO state. At low temperatures, the ground state of YBMO5[15] contains two different types of Mn atoms having simultaneous CO and OO in addition to ferrimagnetic (FI) SO. More complicated behavior has been reported for YBFO5,[2] which undergoes two successive transitions, from the so-called class-III mixed-valence (MV) state (which has a common average charge of 2.5+ for all of the Fe atoms) to the class-II MV premonitory CO state (which has a small distinction between the charge states of the two crystallographically different Fe atoms) to the class-I MV state (which has the two distinct Fe^{2+} and Fe^{3+} formal charge states for Fe). The latter transition apparently triggers a number of changes in the crystal, magnetic, and electronic structures of YBFO5. YBCO5 also exhibits antiferromagnetic (AF) SO as well as CO and OO. The magnetic properties of YBCO5 are expected to be more complex than those of the isostructural compounds involving other transition metals because cobalt in a given valence state can have more than one allowed spin state, e.g., Co^{3+} can have low-spin (LS), intermediate-spin (IS), or high-spin (HS) states. These spin states appear to be quite close in energy, opening up the possibility of spin-state transitions upon a change in temperature or lattice deformation. Likewise, an LS-to-HS transition has been reported in YBCO5 upon cooling.[3] Many experimental[16] and theoretical[17–19] attempts to clarify the exact spin states of Co in YBCO5 have been made.

In this work, we report the results of our density functional theory (DFT) calculations analyzing the magnetic and electronic properties of YBaT$_2$O$_5$ (YBTO5) as a function of d-orbital occupancy. We also attempted to explore the valence and spin states of the T atoms using various techniques. We have performed complete structural optimizations to find out the correct magnetic ground states of the YBTO5 phases. In order to check the effects of strong correlation in these phases, we have performed a set of calculations including Hubbard U parameters. Moreover, spin and orbital magnetic moments were calculated explicitly using accurate methods. Above all, we have formulated a new scheme for visualizing the orbital ordering patterns using energy-projected occupation density matrices of d orbitals. This scheme has enabled us to explain almost all of the structural and magnetic properties of these materials.

II. Crystal and Magnetic Structures

The overall features of the structural arrangements in these YBTO5 phases are the same. The crystal structures are derived from the perovskite type, with ordering of the Y and Ba atoms in alternate layers along c and removal of oxygen exclusively from the Y layer. This creates characteristic apically connected double layers of corner-sharing TO$_5$ square pyramids (Figure 1) that form the backbone of the atomic arrangement perpendicular to the c axis. The actual structural arrangement in the YBTO5 phases varies with T (as reflected in the symmetries of the space groups). Another manifestation is seen in the T−O distances in the coordination polyhedra, which are influenced by the size and, to some extent, charge differences between the Y and Ba constituents. In order to enable a direct comparison of bond parameters in the studied systems, the T−O skeleton is shown in Figure 2.

According to the Goodenough−Kanamori rules,[20] *A*-type AF (hereafter *A*-AF) ordering is expected, with ferromagnetic

(5) Mitchell, J. F.; Argyriou, D. N.; Jorgensen, J. D. In *Colossal Magnetoresistance Oxides*; Tokura, Y. Ed.; Gordon and Breach: Amsterdam, 2000; p 187.
(6) Taskin, A. A.; Lavrov, A. N.; Ando, Y. *Phys. Rev. B* **2005**, *71*, 134414.
(7) Moritomo, Y.; Takeo, M.; Liu, X. J.; Akimoto, T.; Nakamura, A. *Phys. Rev. B* **1998**, *58*, R13334.
(8) Thomas, K. J.; Lee, Y. S.; Chou, F. C.; Khaykovich, B.; Lee, P. A.; Kastner, M. A.; Cava, R. J.; Lynn, J. W. *Phys. Rev. B* **2002**, *66*, 054415.
(9) Hardy, V.; Lees, M. R.; Maignan, A.; Hébert, S.; Flahaut, D.; Martin, C.; Paul, D. M. *J. Phys.: Condens. Matter* **2003**, *15*, 5737.
(10) Vidya, R.; Ravindran, P.; Fjellvåg, H.; Kjekshus, A.; Eriksson, O. *Phys. Rev. Lett.* **2003**, *91*, 186404.
(11) Jahn, H. A.; Teller, E. *Proc. R. Soc. London* **1937**, *A161*, 220.
(12) Vidya, R.; Ravindran, P.; Kjekshus, A.; Fjellvåg, H. *Phys. Rev. B* **2002**, *65*, 144422.
(13) Vidya, R.; Ravindran, P.; Vajeeston, P.; Fjellvåg, H.; Kjekshus, A. *Ceram. Int.* **2004**, *30*, 1993.
(14) Ravindran, P.; Vajeeston, P.; Kjekshus, A.; Fjellvåg, H. *Phys. Rev. B* **2004**, *69*, 092405.
(15) Millange, F.; Suard, E.; Caignaert, V.; Raveau, B. *Mater. Res. Bull.* **1999**, *34*, 1.
(16) Akahoshi, D.; Ueda, Y. *J. Phys. Soc. Jpn.* **1999**, *68*, 736.
(17) Wang, J.; Zhang, W.; Xing, D. Y. *Phys. Rev. B* **2001**, *64*, 064418.
(18) Wu, H. *Phys. Rev. B* **2000**, *62*, R11953.
(19) Kwon, S. K.; Park, J. H.; Min, B. I. *Phys. Rev. B* **2000**, *62*, R14637.
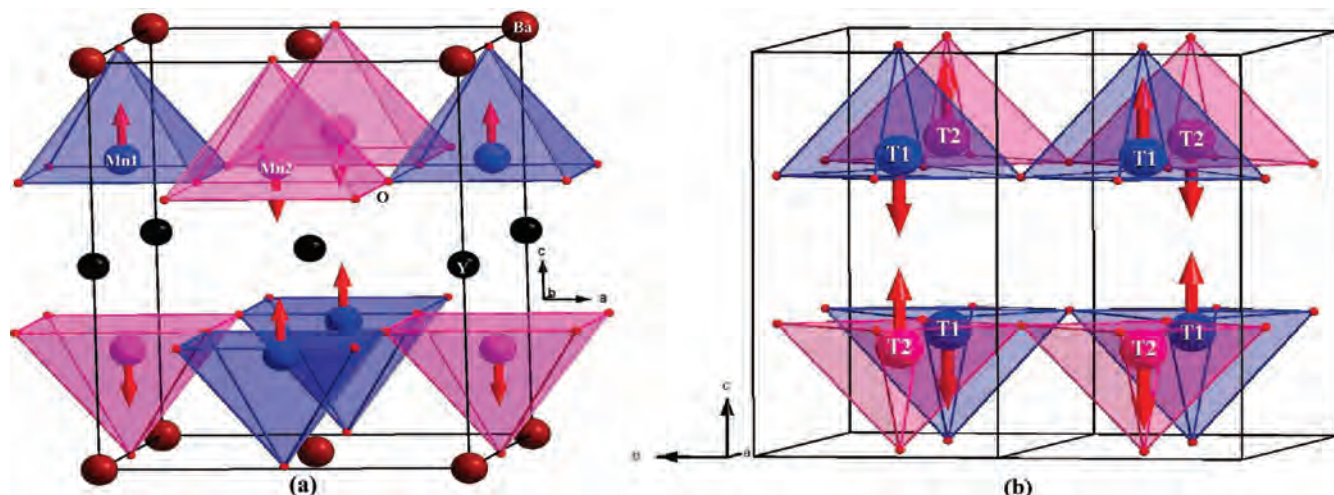
Figure 1. (a) Tetragonal crystal structure of YBaMn$_2$O$_5$ in the AF state, with Y and Ba layers interleaved by MnO$_5$ square pyramids. (b) Wollan−Koehler G-type AF structure of YBaCo$_2$O$_5$ and YBaFe$_2$O$_5$ (Y and Ba atoms are not shown); even though the magnetic moments are oriented along the b axis both experimentally and according to our calculations, here the moments are shown along the c axis in order to facilitate comparison with YBaMn$_2$O$_5$.
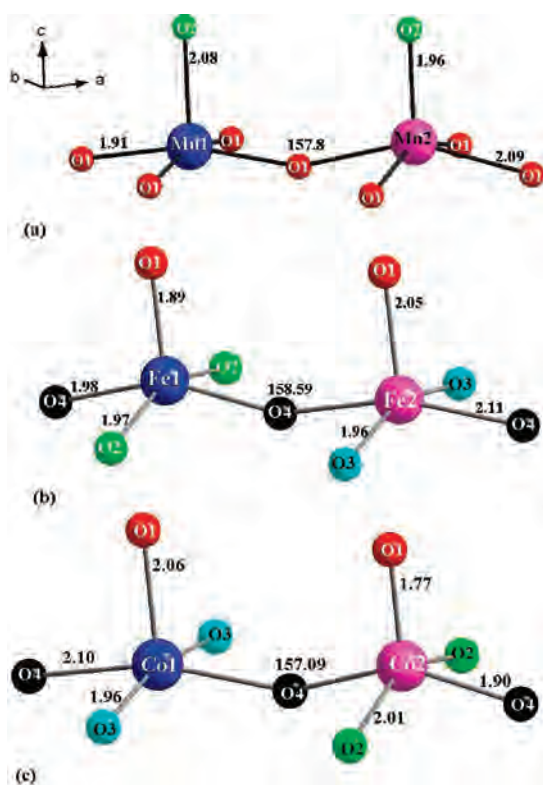
Figure 2. Distortions of the square pyramids in the structures of the YBaT$_2$O$_5$ phases are shown for (a) YBaMn$_2$O$_5$, (b) YBaFe$_2$O$_5$, and (c) YBaCo$_2$O$_5$. T−O bond distances (Å) and pyramid-base-plane T−O−T bond angles (deg) from the optimized structure data are also given.

(F) interactions between T1 and T2 in planes parallel to the ab plane and AF superexchanges along the c direction. However, because of the large deviation of the Mn1−O1−Mn2 angle from 180° in the pyramid-base plane, this interaction also becomes AF in YBMO5, resulting in a G-AF-type magnetic structure that is in fact FI as a result of noncancellation of the differently sized Mn1 and Mn2 moments (see

(20) Goodenough, J. B. *Magnetism and the Chemical Bond*; Interscience: New York, 1966.

Figure 1a). In an effort to check the magnetic-structure postulate, we calculated the total energies of the system in the A-AF and G-AF-type magnetic structures, and the results are discussed in Magnetic Properties−Spin Ordering, below.

YBFO5 converts to class-I MV (space group *Pmma*, with very different nearest-neighbor coordinations and charge states for the Fe atoms) at 20 K. The conversion to class-I MV YBMO5 (space group *Pmmm*) is reported to occur at 1.5 K.[2] The Fe1 site (said to be in a formal Fe^{3+} state) has a fairly symmetric coordination environment at low temperatures, with a slight shift of Fe1 toward the apex of the square pyramid and a consequent shrinkage in the dimensions of the pyramid-base plane to allow shortening of the Fe1−Ob distance, where Ob denotes the oxygen atom at the base of the square pyramid. On the other hand, the coordination of the Fe2 site (formally containing Fe^{2+}) is very distorted, as manifested by the lengthening of the Fe−O bonds in the pyramid-base plane.

The structural features of YBCO5 are similar to those of YBFO5; complete conversion to class-I MV is reported to occur at 50 K.[2] Like YBFO5, class-I MV YBCO5 also exhibits alternating long and short bonds (Co1−O and Co2−O) along a doubled a axis (compared with YBMO5) and chains of either Co1−O−Co1 or Co2−O−Co2 linkages running parallel to b. This change in bond lengths, along with the orthorhombic symmetry, differentiates the CO and OO patterns in YBFO5 and YBCO5 from those in YBMO5. All in all, it is the average noninteger charge state of T and the corner-sharing square-pyramidal framework of the oxygen-deficient perovskite-type structure that set the stage for the CO transition in these materials.

The magnetic structure of YBFO5 also transforms from G-AF-type ordering (of the YBaCuFeO5 type) to a variant denoted as the Wollan−Koehler G-AF-type magnetic arrangement (Figure 1b). In YBFO5 and YBCO5, the isovalent Fe and Co atoms, respectively, arrange themselves in chains, unlike the situation in YBMO5, where a given Mn site has nearest Mn neighbors in a different charge state.[2,3] The

Spin, Charge, and Orbital Ordering in YBaT$_2$O$_5$ (T = Mn, Fe, Co)

Table 1. Optimized Ground-State Structural Parameters for YBaT$_2$O$_5$ Obtained Using VASP (with Experimental Values in Parentheses)

compound	unit cell data[a]	atom	site	x	y	z
YBaMn$_2$O$_5$[b]	a = 5.5643 (5.5359)	Y	2b	$^1/_4$ ($^1/_4$)	$^3/_4$ ($^3/_4$)	$^1/_2$ ($^1/_2$)
	c = 7.6176 (7.6151)	Ba	2a	$^1/_4$ ($^1/_4$)	$^3/_4$ ($^3/_4$)	0 (0)
	V = 235.85 (233.37)	Mn1	2c	$^1/_4$ ($^1/_4$)	$^1/_4$ ($^1/_4$)	0.2760 (0.2794)
	space group P4/nmm	Mn2	2c	$^1/_4$ ($^1/_4$)	$^1/_4$ ($^1/_4$)	0.2582 (0.2514)
		O1	8j	0.4919 (0.4911)	0.4919 (0.4911)	0.3133 (0.3164)
		O2	2c	$^1/_4$ ($^1/_4$)	$^1/_4$ ($^1/_4$)	0.0019 (0.0061)
YBaFe$_2$O$_5$[c]	a = 8.0847 (8.0251)	Y	2c	0 (0)	0 (0)	$^1/_2$ ($^1/_2$)
	b = 3.8373 (3.8383)	Ba	2a	0 (0)	0 (0)	0 (0)
	c = 7.5889 (7.7312)	Fe1	2f	$^1/_4$ ($^1/_4$)	$^1/_2$ ($^1/_2$)	0.2386 (0.2542)
	V = 235.48 (231.98)	Fe2	2f	$^3/_4$ ($^3/_4$)	$^1/_2$ ($^1/_2$)	0.2385 (0.2695)
		O1	2f	$^1/_4$ ($^1/_4$)	$^1/_2$ ($^1/_2$)	0.0001 (0.003)
		O2a	2e	$^3/_4$ ($^3/_4$)	0 (0)	0.3176 (0.3213)
		O2b	2e	$^1/_4$ ($^1/_4$)	0 (0)	0.3172 (0.3132)
		O3	4j	0.0004 (0.0098)	$^1/_2$ ($^1/_2$)	0.3079 (0.3119)
YBaCo$_2$O$_5$[d]	a = 7.7409 (7.8235)	Y	2c	0 (0)	0 (0)	$^1/_2$ ($^1/_2$)
	b = 3.8737 (3.8746)	Ba	2a	0 (0)	0 (0)	0 (0)
	c = 7.5115 (7.4367)	Co1	2f	$^1/_4$ ($^1/_4$)	$^1/_2$ ($^1/_2$)	0.2563 (0.2710)
	V = 225.24 (225.43)	Co2	2f	$^1/_4$ ($^1/_4$)	$^1/_2$ ($^1/_2$)	0.7428 (0.7550)
	space group Pmma	O1	2f	$^1/_4$ ($^1/_4$)	$^1/_2$ ($^1/_2$)	0.0026 (−0.0060)
		O2a	2e	$^1/_4$ ($^1/_4$)	0 (0)	0.6908 (0.6830)
		O2b	2e	$^1/_4$ ($^1/_4$)	0 (0)	0.3127 (0.307)
		O3	4j	0.4941 (0.4847)	$^1/_2$ ($^1/_2$)	0.3115 (0.3105)

[a] Values of a, b, and c are in Å, and values of V are in Å^3. [b] Experimental values from ref 15. [c] Experimental values from ref 2. [d] Experimental values from ref 3.

magnetic structure of YBMO5 contains two formula units, whereas that of YBFO5 and YBCO5 contains four formula units. In the calculations for YBaT$_2$O$_5$ phases in AF configurations, we adopted the appropriate experimental magnetic structures.

III. Computational Details

The present calculations were performed using DFT as implemented in the full-potential linearized augmented-plane-wave (FPLAPW-WIEN2k) method,[21] in a fully relativistic version that includes spin–orbit coupling (SOC). The charge densities and potentials inside the atomic spheres were represented by spherical harmonics up to $l = 6$, whereas in the interstitial region, these quantities were expanded in Fourier series. Atomic-sphere radii, R_{MT}, of 2.2, 2.3, 1.9, and 1.6 au were used for Y, Ba, T, and O, respectively. Since the spin densities are well confined within a radius of about 1.5 au, the resulting magnetic moments do not depend appreciably on the chosen atomic-sphere radii. The initial basis set included 5s, 5p, and 4d valence and 4s and 4p semicore functions for Y, 6s, 6p, and 6d valence and 5s and 5p semicore functions for Ba, 4s, 4p, and 3d valence and 3s and 3p semicore functions for T, and 2s, 2p, and 3d functions for O. The Brillouin zone (BZ) integration was done using a modified tetrahedron method,[22] and we used 168 **k** points in the irreducible wedge of the BZ. Exchange and correlation effects were treated within DFT using the generalized gradient approximation (GGA).[23] Coulomb correlation effects were taken into account by introducing $U = 4.0$ eV and $J = 0.95$ eV for Mn in YBMO5 and $U = 6.0$ eV and $J = 1.0$ eV for Fe and Co in YBFO5 and YBCO5, respectively. In order to calculate the orbital moments accurately, orbital-dependent potentials were

calculated by including orbital polarization (OP).[24,25] The required OP parameters were obtained from ab initio calculations so that no empirical parameters would be included in the calculation, as in the case of GGA+U. The GGA+U[26] and GGA+OP calculations were also carried out using the WIEN2k program.

We also attempted to quantify the amount of charge at each atomic site using Bader's "atom-in-molecule" (AiM) concept[30] and Born effective charges (BECs). While the Bader charges were calculated using the WIEN2k program, the BEC calculations were performed using the Vienna ab initio simulation package (VASP)[27] implementation of the projector-augmented-wave (PAW) method.[22] For the calculation of BECs, the Berry phase approach as adopted for spin-polarized cases was used. We employed basis sets with 700 eV for the plane-wave cutoff and a $4 \times 4 \times 4$ **k**-point mesh. In order to find the insulating states required for the Berry phase calculations, we applied the GGA+U method for YBFO5 and YBCO5 (with $U = 6.0$ and $J = 1.0$ eV) as implemented in the VASP code. In fact, we calculated the total energies and densities of states (DOSs) for different U values ($U = 4.0$, 5.0, and 6.0 eV) and looked for insulating behavior. We obtained an insulating state in YBCO5 only for the above-mentioned U and J values. Hence, we used the same values in the BEC calculations. Moreover, we performed complete structural optimizations for the studied phases using the VASP-PAW method.

IV. Results and Discussion

The optimized crystal-structure parameters obtained after stress and force minimizations were found to be in good agreement with the experimental structural parameters (Table 1).

A. Magnetic Properties—Spin Ordering. In addition to

(21) Blaha, P.; Schwarz, K.; Madsen, G. K. H.; Kvasnicka, D.; Luitz, J. *WIEN2k, An Augmented Plane Waves + Local Orbitals Program for Calculating Crystal Properties*, revised edition 2006; Vienna University of Technology: Vienna, 2006.
(22) Blöchl, P. E. *Phys. Rev. B* **1994**, *50*, 17953.
(23) Perdew, J. P.; Burke, K.; Ernzerhof, M. *Phys. Rev. Lett.* **1996**, *77*, 3865.
(24) Brooks, M. S. S. *Phys. B* **1985**, *130*, 6.
(25) Eriksson, O.; Johansson, B.; Brooks, M. S. S. *J. Phys. C* **1989**, *1*, 4005.
(26) Novak, P.; Boucher, F.; Gressier, P.; Blaha, P.; Schwarz, K. *Phys. Rev. B* **2001**, *63*, 235114.
(27) (a) Kresse, G.; Hafner, J. *Phys. Rev. B* **1993**, *47*, 558. (b) Kresse, G.; Furthmuller, J. *Comput. Mater. Sci.* **1996**, *6*, 15.

Table 2. Total Energies (meV per formula unit) for YBaT$_2$O$_5$ in the NM, F, and AF States[a]

phase	NM	F	AF
YBaMn$_2$O$_5$	3388	422	0
YBaFe$_2$O$_5$	2588	967	0
YBaCo$_2$O$_5$	873	428	0

[a] Total energies are relative to that of the lowest-energy state. The calculations were performed using the Wien2k code and included GGA and SOC. YBaFe$_2$O$_5$ and YBaCo$_2$O$_5$ have Wollan−Koehler G-AF-type structures.

confirming the experimentally determined AF structures, we performed calculations for the nonmagnetic (NM), F, and AF configurations and established that these three compounds have AF ground states (Table 2). Because the Goodenough−Kanamori rules suggest an A-AF-type structure for YBMO5, we also calculated the total energy for this arrangement. However, the calculated total energy was 124 meV per formula unit higher than that for the ground-state G-AF-type structure. The magnetic moments at the two Mn sites were different (3.28 and 3.82μ_B, respectively) in the A-AF configuration of YBMO5 and had perfect AF arrangement. On the other hand, the magnetic moments for the two Mn sites in the G-AF-type configuration (see Table 3) did not cancel, resulting in an FI configuration in agreement with the experimental findings.[15] In the case of YBMO5, the effect of SOC on the calculated magnetic moments of the Mn atoms was negligible. It is interesting to note that while GGA+U overestimated the spin magnetic moments, GGA+OP provided magnetic moments in very good agreement with the experimental values.

In the GGA+SOC calculations, the difference in the calculated magnetic moment values for the Fe sites in YBFO5 was small. The increased difference between the magnetic moments when we included Coulomb correlation effects in the calculation ($U = 6.0$ eV and $J = 1.0$ eV) implies that correlation effects play an important role in YBFO5. Even though the experimental Rietveld refinements[2] were able to distinguish two different coordination environments for the Fe sites, powder neutron diffraction measurements were unable to establish different magnetic moments for these two Fe atoms. However, our theoretical calculations were able to confirm different magnetic moments for the Fe sites. In fact, the magnetic moment value found for the Fe1 site is in good agreement with the reported experimental value (Table 3). The orbital magnetic moments of the Fe atoms were negligibly small, as was the case for Mn in YBMO5.

The magnetization curve for YBCO5 showed an anomaly at ∼340−350 K that was attributed to the onset of AF spin ordering.[3] The experimental study also clearly established distinct magnetic moments for the Co sites, which have an AF configuration similar to that in YBFO5. As seen from Table 3, inclusion of correlation effects increased the difference between the moments at the Co1 and Co2 sites. When orbital moments were also added, a somewhat good agreement with the experimental values was obtained. The calculated orbital moments of 0.01 and 1.01μ_B for the Co1 and Co2 sites, respectively, are close to the values of 0.04 and 1.04μ_B, respectively, obtained earlier using an LDA+U

calculation.[19] Among the three studied systems, YBCO5 has a significant orbital moment at the Co2 site. The calculated magnetic moments at the Co1 and Co2 sites using GGA+OP (2.06 and 3.42μ_B, respectively) are comparable with the results of other theoretical studies (2.80 and 3.20μ_B from ref 18 and 2.24 and 3.65μ_B from ref 19). The calculated moments at the Co sites are in good agreement with those in the isostructural HoBaCo$_2$O$_5$ phase.[28] It should be noted that 9% of the total moment per formula unit originated from induced moments at the oxygen sites. Among the various computational techniques used for the estimation of magnetic moments, we found that the GGA+OP method gave an overall good agreement with experimentally determined magnetic moments.

It is of interest to analyze why YBMO5 exhibits simple G-AF-type magnetic ordering but YBFO5 and YBCO5 have Wollan−Koehler G-AF-type ordering in spite of the fact that all three compounds have essentially the same atomic frameworks. One of the main reasons for this difference is the variation in OO exhibited by the transition-metal d orbitals (see Orbital Ordering, below).

B. Electronic Structure. In order to analyze the electronic structures of the YBaT$_2$O$_5$ phases, we plotted total as well as site- and orbital-projected densities of states. In its NM state, each of the three compounds had a finite number of states at E_F, indicating metallic character. Moreover, E_F fell on a peak in the total DOS for each of the YBTO5 phases, suggesting instability of these phases in the NM state, in agreement with the total-energy studies. In YBCO5, a pronounced upturn in the resistivity near 200 K has been reported;[3] this is indicative of electron localization that could be associated with CO on the cobalt sites. The change in resistivity may be taken as an indicator of metallic character in the NM state of YBCO5, in agreement with our calculations and an unrestricted Hartree−Fock calculation.[29] The DOS for the F state in each of the three phases revealed metallic character but a considerably reduced number of states at E_F compared with the NM case.

YBMO5 is a semiconductor in the FI ground state, with an energy gap (E_g) of 0.88 eV (Figure 3) between the valence band (VB) and the conduction band (CB). The GGA+SOC calculation itself reproduced the correct insulating behavior of YBMO5 at 0 K. When the Coulomb correlation effect was included in the calculation ($U = 4.0$ eV and $J = 0.95$ eV), the value of E_g increased to 1.42 eV (see the top panel of Figure 3).

The GGA-type calculations without SOC for YBFO5 and YBCO5 resulted in DOSs with finite numbers of states at E_F (not shown). However, when SOC was included, some stability was obtained, in the sense that E_F fell on a pseudogaplike feature for both phases (Figure 3). The total DOSs obtained from GGA+U calculations for YBFO5 and YBCO5 (Figure 3) exhibited very small energy gaps ($E_g = 0.11$ and

(28) Suard, E.; Fauth, F.; Caignaert, V.; Mirebeau, I.; Baldinozzi, G. *Phys. Rev. B* **2000**, *61*, R11871.
(29) Wang, J.; Tao, Y. C.; Zhang, W.; Xing, D. Y. *Phys. Rev. B* **2002**, *65*, 052402.
(30) Bader, R. F. W. *Atoms in Molecules−A Quantum Theory*; Clarendon Press: Oxford, U.K., 1990.

Table 3. Calculated Spin and Orbital Magnetic Moments (μ_B per T atom) for YBaT$_2$O$_5$ in the AF Ground State

	YBMO5			YBFO5			YBCO5		
method	Mn1	Mn2	total[a]	Fe1	Fe2	total[a]	Co1	Co2	total[a]
GGA	2.94	3.79	0.85	3.46	3.34	0.00	2.30	2.68	0.00
GGA+SOC (spin)	2.96	3.78	1.00	3.32	2.96	0.00	1.94	1.98	0.00
GGA+SOC (orbital)	0.01	0.04	–	0.03	0.01	–	0.04	0.28	–
GGA+U (spin)	3.21	4.06	0.99	3.71	3.16	0.00	1.66	2.51	0.00
GGA+U (orbital)	0.00	0.00	–	0.00	0.00	–	0.01	1.01	–
GGA+OP (spin)	2.94	3.78	0.99	3.32	2.96	0.00	1.97	1.98	0.00
GGA+OP (orbital)	0.04	0.01	–	0.08	0.07	–	0.09	1.44	–
experimental	2.90[b]	3.90	0.95	3.82[c]	–	0.0	2.70[d]	4.20	0.0

[a] Total magnetic moment per formula unit. [b] From low-temperature neutron diffraction, ref 15. [c] From low-temperature neutron diffraction, ref 2. [d] From low-temperature neutron diffraction, ref 3.
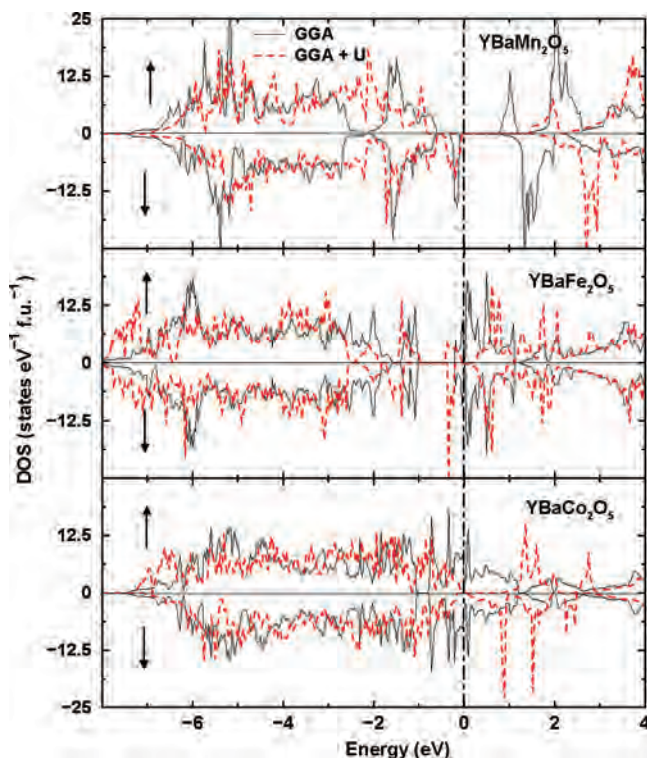
Figure 3. Total densities of states of YBaT$_2$O$_5$ (T = Mn, Fe, Co) in their ground-state (*G*-AF) magnetic configurations (see Table 1) obtained using the GGA+SOC (black solid line) and GGA+U (red dashed line) methods.

0.13 eV, respectively). References 19 and 29 reported insulating behavior for the AF state of YBCO5 upon inclusion of LSDA+U in the calculations.

Since the site-projected DOSs for the different YBTO5 phases were very similar, we have displayed only those for YBFO5 and YBCO5 from the GGA+U calculations (Figure 4). The Y and Ba sites exposed few states in the VB compared with the CB, indicating that the Y and Ba atoms have lost their valence electrons to the O constituents. The two distinct T sites have topologically different DOS features, immediately signaling a possible MV situation. Even though d states were seen from −8 to −2 eV for Fe1 (Figure 4a), significant bonding states were far (−8 to −6.5 eV) from E_F. On the other hand, Fe2 had significant states across the entire energy region of the VB, from −7 to −1 eV. Moreover, the minority-spin channel of Fe1 was almost empty, whereas Fe2 had significant minority-spin states closer to E_F. This concurs with the fact that Fe1 had a larger magnetic moment than Fe2. Co1 in YBCO5 had significant

majority- as well as minority-spin states, reducing the exchange interaction and thus the magnetic moment at the Co1 site (Figure 4b). On the other hand, the minority-spin channel of Co2 contained considerably fewer states than that of Co1. Therefore, a larger magnetic moment is observed at the Co2 site than at the Co1 site. The different types of oxygen atoms exhibited topological differences over the energy range −8 to −2 eV. As d states of T also existed in the same energy range, covalent hybridization interactions between d states of T and p states of O can be envisaged, providing one of the reasons for the decrease in the spin magnetic moments of the T atoms compared with the pure ionic case.

Figure 5 displays DOSs for the d states of the T atoms in their respective YBTO5 ground-state configurations. Among the three phases, sharp peaks in the Mn d states of YBMO5 were seen in the energy range −2 to 0 eV. In YBFO5, the effect of GGA+U was to make the Fe2 minority-spin states more localized, thereby introducing semiconducting behavior with a finite energy gap. The DOS profiles suggest that the d electron added upon going from YBMO5 to YBFO5 should have entered the majority-spin band, resulting in an increased difference between the majority- and minority-spin bands and, subsequently, in higher magnetic moments for both sites. The influence of GGA+U on YBCO5 was mainly focused on the electrons in the energy range −2 to 0 eV, which are pushed down (away) from E_F. When Co replaced Fe in going from YBFO5 to YBCO5, the states closer to E_F may have received the added extra electron. Hence, this change appeared to have negligible magnetic consequences but increased the bonding interactions. As a result, the Co 3d states in YBCO5 are relatively delocalized.

C. Charge Ordering. 1. Charge States. According to ref 2, the bond valence sums (BVSs) for Mn1 and Mn2 in YBMO5 are 2.43 and 3.10, respectively; the corresponding BVS values are 2.23 and 2.94 for Fe in YBFO5 and 2.02 and 2.69 for Co in YBCO5. The different BVS values for different T atoms are indications of different charge states. Moreover, the valence charge densities within the *ac* planes of the YBaT$_2$O$_5$ phases (Figure 6) showed that the amounts of charge in the T1−O and T2−O bonds were different, providing additional evidence that the actual charge states of the T atoms differ. Because of their shorter bond lengths, the Mn2−Oa bond is stronger than the Mn1−Oa bond whereas the Mn1−Ob bonds are stronger than the Mn2−Ob bonds (Oa and Ob refer to oxygen atoms at the apex and
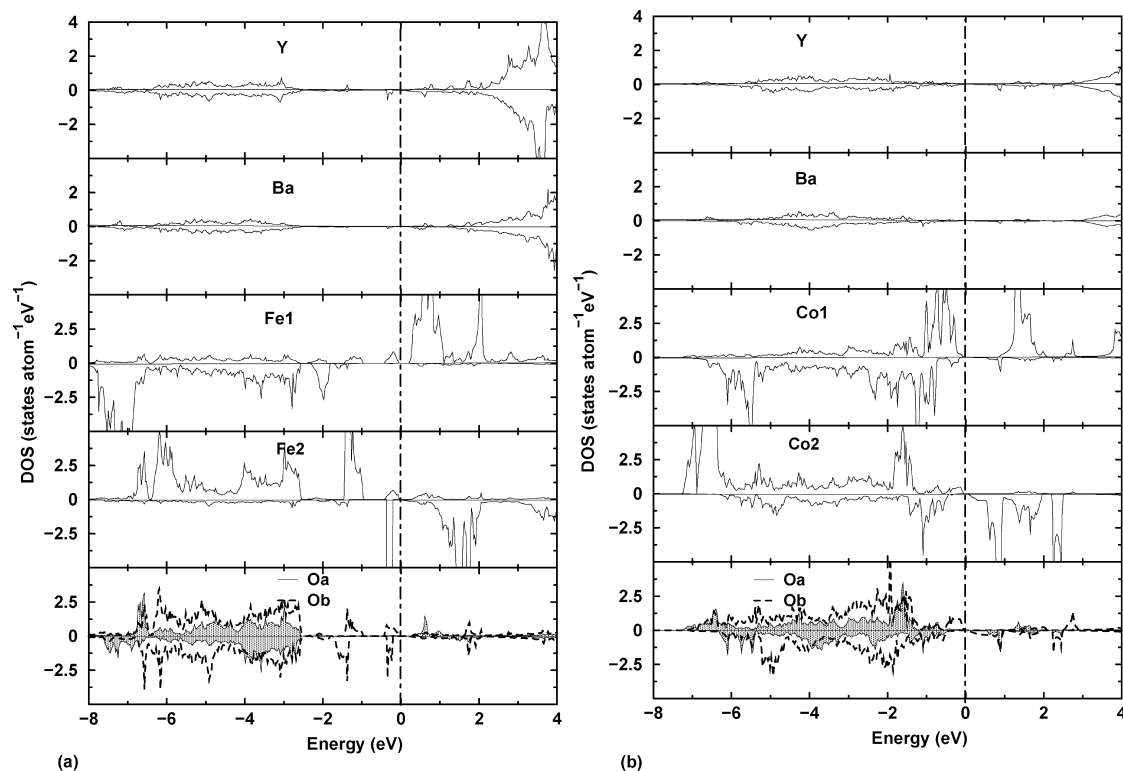
Figure 4. Site-projected densities of states for (a) YBaFe$_2$O$_5$ and (b) YBaCo$_2$O$_5$ in the AF configuration. Coulomb correlation effects were included in the calculations. Oxygen atoms at the apex and base of the square-pyramidal coordination are denoted as Oa and Ob, respectively; shaded regions refer to DOS for Oa atoms.
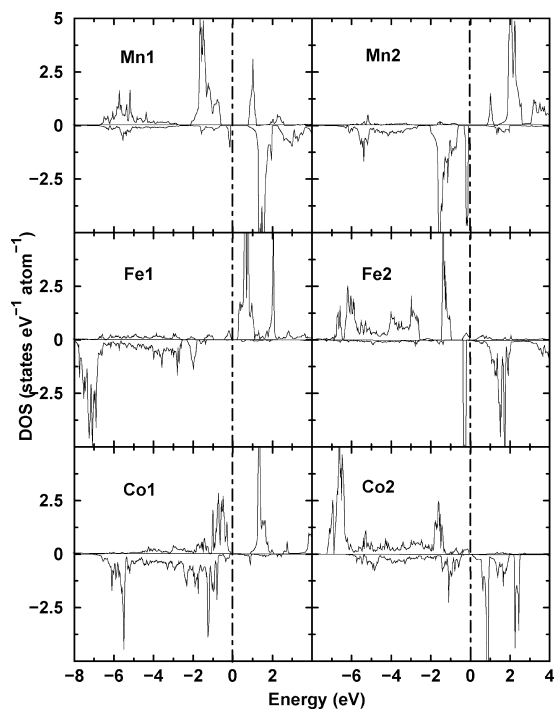

Figure 5. Site-projected densities of states for the T sites in YBMO5, YBFO5, and YBCO5.

base of the square pyramids, respectively). Similarly, the Fe1−Ob bonds are stronger than the Fe2−Ob bonds. However, the opposite is true for YBCO5, which has stronger Co2−Ob bonds than Co1−Ob bonds, since the Co2−Ob bond lengths along the *a* and *b* directions are shorter than

the Co1−Ob bond lengths (see Figure 2c). Overall, the T−Oa bonds seem to be stronger than the T−Ob bonds, and the Co2−Oa bonds seem to be stronger than the Mn2−Oa and Fe2−Oa bonds. Thus, the charge-density analysis established different bonding characteristics for the T atoms of the YBaT$_2$O$_5$ phases and hence localization of different amounts of charge on the different T1 and T2 atoms, which in turn leads to CO.

2. Bader Charge Analysis. In an effort to assign more-proper charge states to the T atoms in the YBaT$_2$O$_5$ phases, we attempted to quantify the charges at the atomic sites using various techniques. We first made use of the AiM concept of Bader,[30] which divides space into regions using surfaces that run through minima in the charge density. The appropriate regions are chosen such that the gradient of the charge density at any location on the bordering surface has no component normal to the surface. A region enclosed by such boundary surfaces is called a Bader region. Integrating the charge density within the Bader region where a given atom's nucleus is located and adding electronic charges in "naturally associated neighboring regions" that do not include a nucleus yield an estimate of the total excess charge on that atom. The advantage of this method is that the analysis is based solely on the charge density, so the results are rather insensitive to the basis set used in the calculation of the charge distribution.

The calculated Bader charges in Table 4 lend further support to the inference that the T1 and T2 sites in these phases exhibit different charges. However, we must admit that this approach was not able to provide quantitative
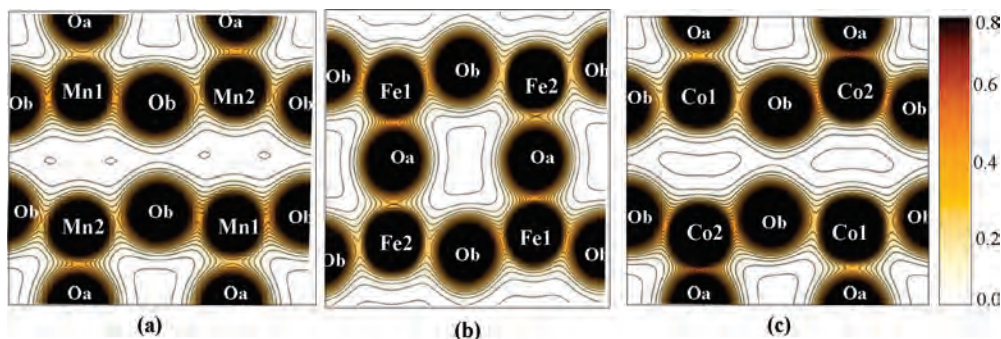
Figure 6. Valence charge densities within the *ac* plane for (a) YBaMn₂O₅, (b) YBaFe₂O₅, and (c) YBaCo₂O₅. Atoms are labeled in the illustration, and oxygen atoms at the apex and base of the square-pyramidal coordination are denoted as Oa and Ob, respectively. Note that the map in panel b is somewhat shifted compared to those in panels a and c.

Table 4. Calculated Bader Charges q_B and Net Ionic Charges Δq_B inside Regions Defined by the Bader AiM Concept, As Implemented in the Wien2k Code[a]

	YBMO5		YBFO5		YBCO5	
element	q_B	Δq_B	q_B	Δq_B	q_B	Δq_B
Y	37.58	+1.42	36.84	+2.16	37.53	+1.47
Ba	54.90	+1.10	54.48	+1.52	54.82	+1.18
T1	24.15	+0.85	24.48	+1.52	26.35	+0.65
T2	24.41	+0.59	24.72	+1.28	26.23	+0.77
O1	8.80	−0.80	9.27	−1.27	8.78	−0.78
O2	8.73	−0.73	9.31	−1.31	8.80	−0.80

[a] $\Delta q_B = q_Z - q_B$, where q_Z is the electronic charge in the corresponding neutral atom. All values are in units of *e*.

assessments of the charge states of the T atoms. The root of the problem was the mixture of ionic and covalent bonding in these phases, a feature that involves not only the T atoms. The conceptual shortcomings were also reflected in the Bader net ionic charges residing in the Y and Ba regions, which certainly do not correspond to the ionic charges of 3+ and 2+, respectively, obtained from simple electron accounting, and also those in the O regions, which indicate that O does not exhibit a completely filled valence shell (i.e., that it is not O^{2-}). However, we presume that even the small charge distinctions exposed in Table 4 could have been large enough to occasion CO (see Calculation of the Born Effective-Charge Tensor, below). The difference between the Bader charges for Mn1 and Mn2 (0.26) exceeds those for Fe1 and Fe2 (0.24) and Co1 and Co2 (0.12), which may provide a hint as to why the CO transition temperature is higher (and the CO effect is more pronounced) for YBMO5 than for YBFO5 and YBCO5.[2]

3. Calculation of the Born Effective-Charge Tensor. Another useful tool to quantify charges is the BEC tensor, which provides the polarized charges induced by application of an electric field.[32] Hence, we attempted to calculate BEC tensors using the Berry phase approach as implemented in the VASP-PAW method. A detailed description of the calculation of the BEC tensor is provided elsewhere.[31] As the Berry phase calculation requires an insulating state, we searched for such states using the GGA+*U* approach for YBFO5 and YBCO5 and the usual GGA method for

YBMO5. Unfortunately, we were unable to obtain the insulating state for YBFO5 using the VASP code, though we obtained a small band gap using the Wien2k calculation. We even tried using different *U* values (4.0, 5.0, 6.0, 7.0, and 8.0 eV), but none of these calculations yielded insulating behavior for YBFO5. The failure of VASP to observe semiconducting behavior for YBFO5 may be associated with that phase's small band gap value, which is within the predicting capability of this code or the more extended basis set involved in the VASP calculation. An insulating state for YBCO5 was obtained with $U = 6.0$ eV and $J = 1.0$ eV, and accordingly, these parameters were used in the BEC calculations. The diagonal components of the BEC tensors for YBMO5 and YBCO5 and their average values are listed in Table 5.

The anisotropic diagonal components and finite off-diagonal components (not given) of the BEC tensors clearly indicated the presence of covalent bonding interactions. A closed-shell ion should carry an effective charge close to its nominal ionic value. On the contrary, a large amount of nonrigid delocalized charge flows across the skeleton of a compound with covalent bonds when the lattice is subjected to displacement.[33] Hence, one usually obtains BEC components larger than the nominal ionic values. In view of these facts and the iono-covalent nature of the bonding, Y in YBMO5 can (to a zeroth approximation) be assigned a charge of 3+, and Ba, Mn1, Mn2, and O can correspondingly be assigned charges of 2+, 3+, 2+, and 2−, respectively. Similarly, Y and Ba in YBCO5 can be assigned charges of 3+ and 2+, respectively. Since the average value of the diagonal elements of the BEC tensor for Co1 was close to 2, Co1 can be inferred to have a charge of 2+ and Co2 correspondingly to be in the 3+ state. Since the numerical average of the diagonal BEC-tensor elements for all types of O atoms in YBCO5 was slightly larger than 2, O atoms can be assigned a 2− charge. Since the magnetic and electronic properties of YBFO5 are similar to those of YBCO5, the constituents of YBFO5 can be assigned charges in conjunction with those of YBCO5, i.e., Y, Ba, and O can be assigned charges of 3+, 2+, and 2−, respectively, and the Fe atoms charges of 3+ and 2+, in line with those in

(31) Ravindran, P.; Vidya, R.; Kjekshus, A.; Fjellvåg, H.; Eriksson, O. *Phys. Rev. B* **2006**, *74*, 224412.

(32) (a) Martin, R. M. *Phys. Rev. B* **1974**, *9*, 1998. (b) Pick, R.; Cohen, M. H.; Martin, R. M. *Phys. Rev. B* **1970**, *1*, 910.

(33) Zhong, W.; King-Smith, R. D.; Vanderbilt, D. *Phys. Rev. Lett.* **1994**, *72*, 3618.

Table 5. Calculated Diagonal Elements Z_{ij}^* of the Born Effective-Charge Tensors for YBaMn$_2$O$_5$ and YBaCo$_2$O$_5$ in Their Ground-State Configurations

	YBaMn$_2$O$_5$				YBaCo$_2$O$_5$			
atom	Z_{xx}^*	Z_{yy}^*	Z_{zz}^*	average	Z_{xx}^*	Z_{yy}^*	Z_{zz}^*	average
Y	3.913	3.913	4.169	3.998	3.667	3.662	4.724	4.018
Ba	2.926	2.925	2.612	2.821	3.345	1.969	2.477	2.662
T1	3.745	3.745	1.646	3.046	1.673	2.393	1.504	1.857
T2	2.585	4.586	1.789	2.320	4.688	3.932	1.693	3.437
O1	−2.811	−2.810	−1.624	−2.415	−2.579	−2.222	−2.352	−2.384
O2	−1.919	−1.919	−3.686	−2.508	−2.687	−2.220	−2.352	−2.420
O3	−	−	−	−	−2.737	−2.173	−1.961	−2.291

YBCO5. It can be noted that the charges of the different constituents of YBaT$_2$O$_5$ inferred from the ab initio method in this way are in good agreement with the formal valence assignments for the atoms concerned. Because of the different charges associated with the T atoms, the charges on these atoms are subject to CO below a certain temperature (T_{CO}). While the charges on Mn1 and Mn2 are arranged in a checkerboard-type pattern of CO, those on Fe1 and Fe2 in YBFO5 and Co1 and Co2 in YBCO5 form a stripe-type pattern. One of the main reasons for this distinction is the different types of orbital ordering adopted by the d orbitals of the various T atoms, as discussed in the next section.

D. Orbital Ordering. According to the rigid-band picture, YBMO5 can be converted into YBFO5 by adding one electron to each of the Mn atoms, and YBCO5 can be obtained by adding two electrons to each of the Mn atoms. Hence, it is interesting to see how OO would evolve by progressive filling of the d orbitals of the T atoms. Since there were practical difficulties in adding one electron to Mn in YBMO5, we subtracted one electron from each Co in YBCO5 to make YBFO5 and then subtracted additional electrons to convert YBFO5 into YBMO5. Figure 7 shows how the OO patterns for YBMO5 and YBFO5 would evolve from the OO in YBCO5 according to such a pure rigid-band approach. In YBMO5, the d$_{xz}$ orbital on Mn1 and a combination of the d$_{xz}$, d$_{yz}$, and d$_{xy}$ orbitals on Mn2 should be ordered. In YBFO5, on the other hand, d$_{xz}$ on Fe1 and d$_{xy}$ on Fe2 should be ordered according to the rigid-band picture. Now let us see how the OO evolves in the actual situation.

Since electrons in the vicinity of E_F participate in conduction and play a decisive role in magnetic exchange interac-

tions, we used integrated values of the orbital-projected DOS in a narrow energy range close to E_F (for practical reasons, we chose the interval −1 to 0 eV) to assess OO in earlier studies[12–14] on similar phases. However, in an attempt to make our computational efforts point more directly at the actual situation in the materials under investigation, in this work we tested an alternative approach based on the energy-projected density matrices of the d orbitals of the T constituents.

The starting point was the ground-state charge density, from which the 5×5 occupation-density matrix for the 3d orbital was derived. The occupation matrix for the chosen narrow energy window close to E_F was then fed into the appropriate d orbitals (specified by their functional dependencies and fixed to the constraints of the crystal structure). It should be noted that the shapes of the crystal orbitals resemble their free-atom shapes only when there is no energy overlap with other orbitals. The next step was to look for localized states near E_F using the orbital-projected DOSs as guides and then to identify the orbitals concerned. This procedure provided not only the OO pattern but also a pictorial illustration of the special orientation of a particular d orbital and its degree of filling. This should in principle give more appropriate OO information.

1. YBaMn$_2$O$_5$. According to the orbital-projected DOS for the Mn d orbitals in YBMO5, the d$_{z^2}$ orbital on Mn1 and the d$_{z^2}$ and d$_{x^2-y^2}$ orbitals on Mn2 had energies in the range −1 to 0 eV. In order to evaluate the above-mentioned alternative approach, we first made an OO mapping for YBMO5, the outcome of which is shown in Figure 8a. This illustration demonstrates that the d$_{z^2}$ orbital on Mn1 and the
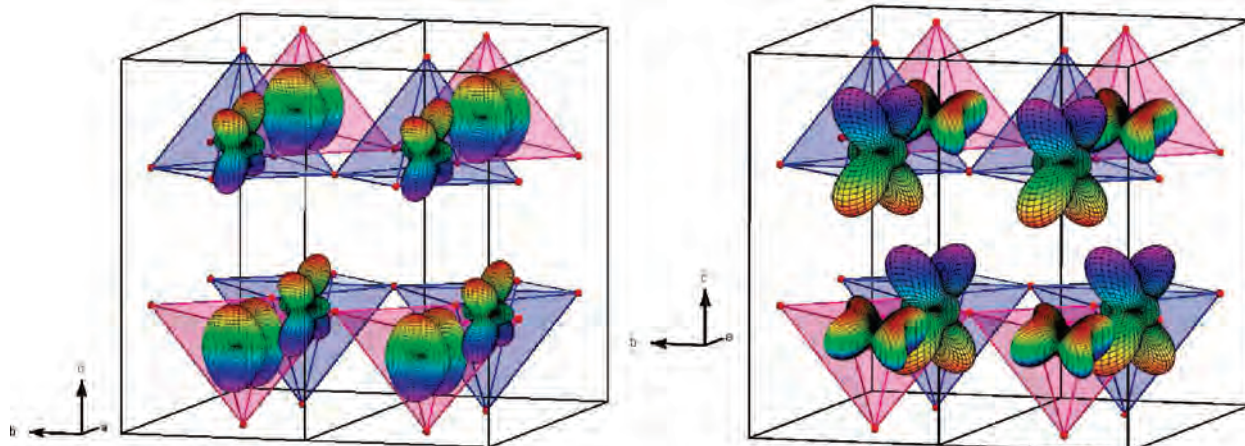
Figure 7. Orbital ordering pattern in (left) YBMO5 and (right) YBFO5 emerging from rigid-band considerations, using YBCO5 as the starting point. In both phases, pseudo-t$_{2g}$ orbitals are seen to be ordered, whereas in reality, the ordering is as shown in Figure 8. Y and Ba atoms have been omitted for clarity.
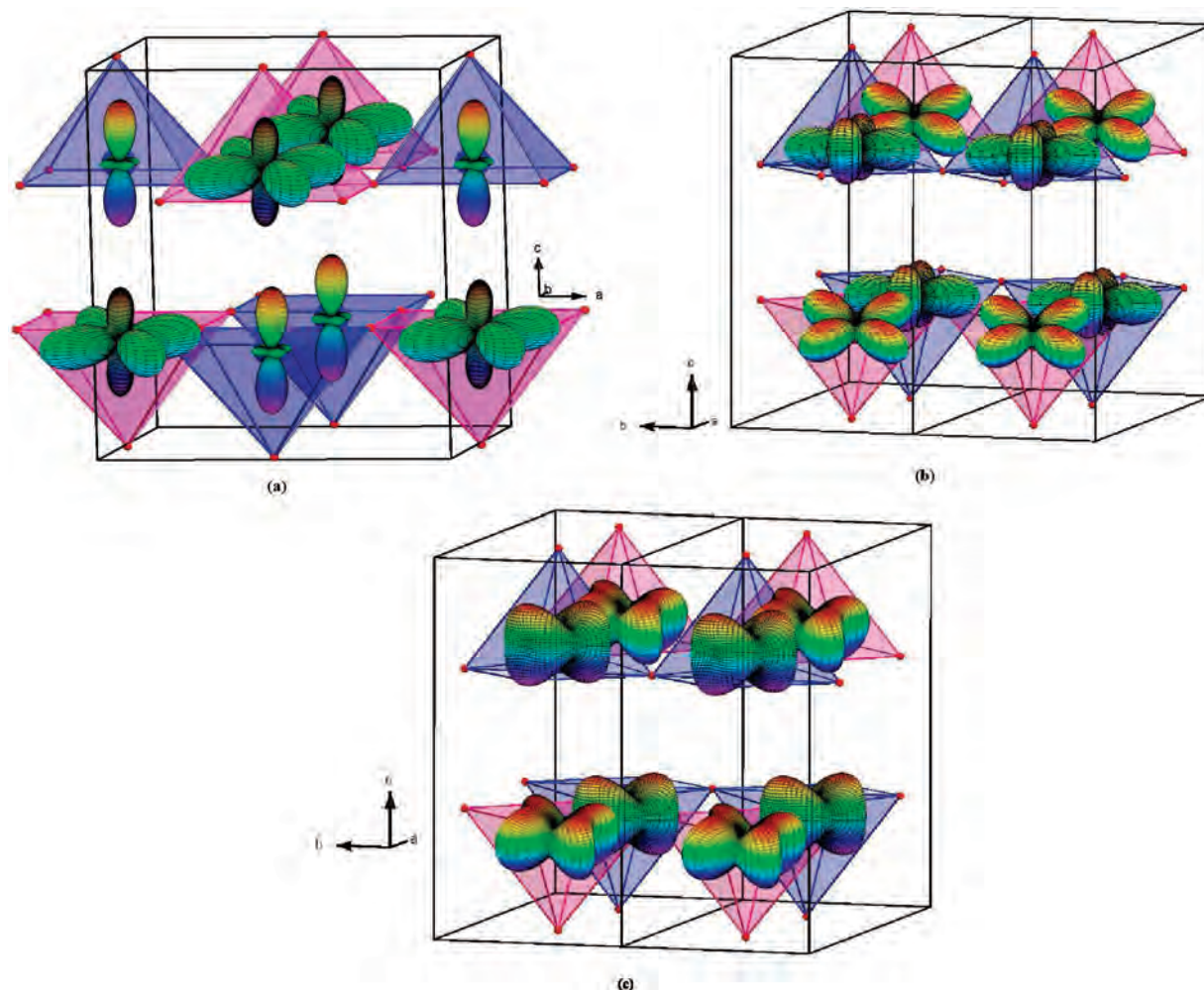
Figure 8. Orbital ordering patterns in (a) YBMO5, (b) YBFO5, and (c) YBCO5, as derived from full-potential calculations. In YBMO5, the d$_{z^2}$ orbital of Mn1 and the d$_{z^2}$ and d$_{x^2-y^2}$ orbitals of Mn2 are ordered, whereas in YBFO5, the d$_{x^2-y^2}$ orbital on Fe1 and the d$_{xz}$ orbital on Fe2 are ordered. In YBCO5, the d$_{xz}$, d$_{yz}$, and d$_{x^2-y^2}$ orbitals on Co1 are ordered, whereas the d$_{yz}$ and d$_{xy}$ orbitals on Co2 are ordered. The blue and pink polyhedra have T1 and T2, respectively, as their central atoms. Y and Ba atoms have been omitted for clarity.

d$_{z^2}$ and d$_{x^2-y^2}$ orbitals on Mn2 are ordered alternatively, in agreement with our earlier findings (see Figure 1d in ref 13). Because of the Mn1−Oa−Mn2 bond angle of 180° along the *c* direction, the Mn1(d$_{z^2}$)−O(p$_z$)−Mn2(d$_{z^2}$) hybridization reaches a maximum. This enables p−d σ bonding as well as AF superexchange interactions in the *c* direction. Because of symmetry constraints, the magnetic moments of Mn1 and Mn2 are antiferromagnetically aligned within the *ab* plane, leading to a simple *G*-AF-type magnetic structure. Since both the d$_{x^2-y^2}$ and d$_{z^2}$ orbitals on Mn2 are ordered, the Mn2−Ob bond length is elongated along *a* and *b* compared to that of Mn1−Ob. The hybridization interaction between the d$_{z^2}$ orbital of Mn1 and the d$_{x^2-y^2}$ orbital of Mn2 reaches a minimum within the *ab* plane because of the different orientations of these orbitals. In addition, the Mn1−Ob−Mn2 bond angle of 157.8° makes the superexchange pathway less effective within the *ab* plane. Therefore, more charges are localized on Mn2 than on Mn1, leading to different magnetic moments at the Mn1 and Mn2 sites and hence the FI ordering and checkerboard-type CO rule in YBMO5. The fact that the Mn1−Ob−Mn2 bond angle is less than 180° is the main reason for the *G*-AF ordering. A model calculation using an

assumed value of 180° for the Mn1−Ob−Mn2 angle resulted[34] in *A*-AF-type ordering that was, however, higher in energy than the *G*-AF-type arrangement.

The orbital-projected DOSs for Mn1 show that four of the five d orbitals are singly occupied on Mn1, whereas all five orbitals are singly occupied on Mn2. On the basis of the above-inferred OO patterns and the charge density shown in Figure 6a (where greater charge is seen on Mn2 than on Mn1), Mn1 can be formally associated with an HS Mn^{3+} state and Mn2 with an HS Mn^{2+} state. This is consistent with the observed magnetic moments at the Mn1 and Mn2 sites as well as the deductions from the BEC tensor calculations. It is interesting to recall that Mn^{3+} in LaMnO$_3$ leads to JTD, whereas no JTD is observed for Mn1 in YBMO5. It should be noted that Mn in LaMnO$_3$ is octahedrally coordinated with its O neighbors, and therefore, the Mn d orbitals are split into triply degenerate t$_{2g}$ and doubly degenerate e$_g$ orbitals. In Mn^{3+} (which has a d^4 configuration), one of these e$_g$ orbitals is singly occupied,

(34) Xiang, H. P.; Liu, X. J.; Wu, Z. J.; Meng, J. *J. Phys. Chem. B* **2006**, *110*, 2606.
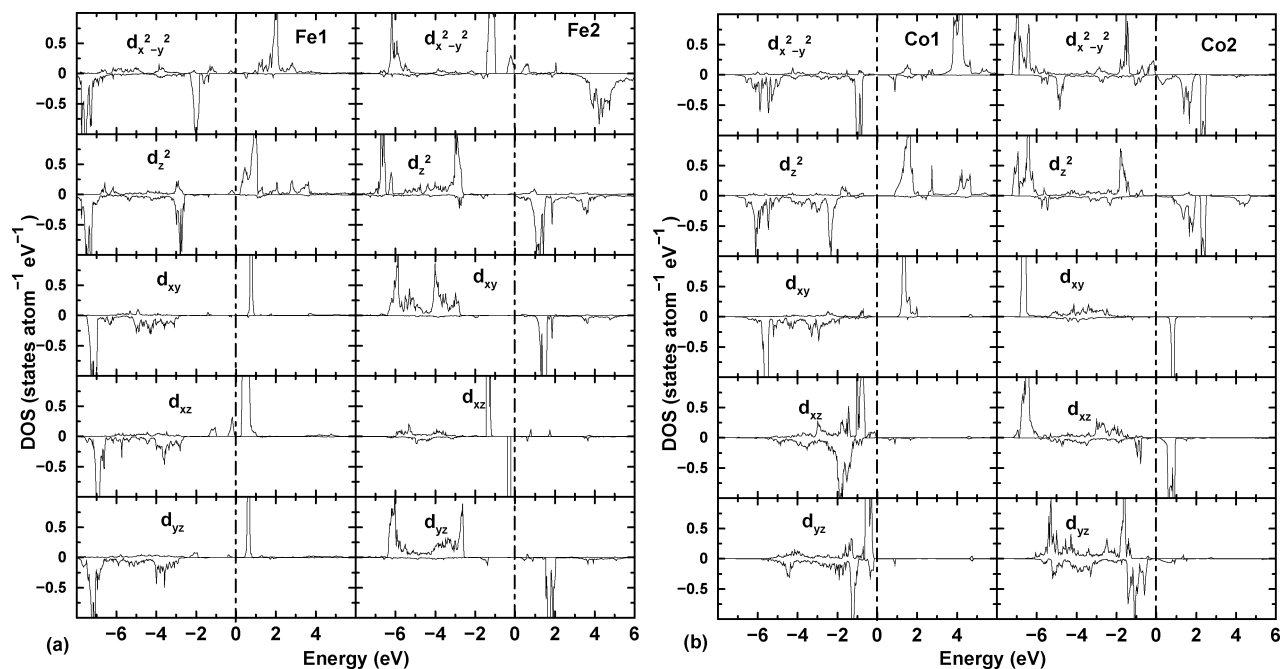
Figure 9. Orbital-projected densities of states for the d orbitals of T in (a) YBaFe₂O₅ and (b) YBCo₂O₅.

leading to JTD and OO in LaMnO₃.[35] On the other hand, the d orbitals on T atoms having square-pyramidal coordination are split into doubly degenerate e_g (d_{xz}, d_{yz}) and nondegenerate b_{2g} (d_{xy}), a_{1g} (d_{z^2}), and b_{1g} ($d_{x^2-y^2}$) levels.[36] As the higher-lying a_{1g} and b_{1g} orbitals are already nondegenerate as a result of crystal-field effects, further JTD is not needed to lift the degeneracy of Mn³⁺ in YBMO5. We performed additional analysis of the orbital-projected DOSs for the Mn d orbitals in the F (metallic) case and found that in both of the Mn atoms, three of the five d orbitals are singly occupied and two are only partially occupied. Unlike the FI case, the d orbitals are prominently spread out over the energy range from −3 to −1 eV. Moreover, the d_{z^2} and d_{xy} states closer to E_F do not exhibit sharp peaks but instead have rather broad features. This implies that YBMO5 does not exhibit OO in the higher-energy (excited-state) F case. Therefore, it can be inferred that the ordering of orbitals in the FI case is the main cause for CO and SO as well as the insulating behavior of YBMO5. As the OO pattern plotted using the new approach based on density matrices was consistent with our earlier deductions as well as the experimentally established magnetic and structural properties, we applied the same procedure to explore the OO in YBFO5 and YBCO5.

2. YBaFe₂O₅. From Figure 9a, it can be seen that Fe1 has five singly occupied d orbitals whereas Fe2 has four singly occupied d orbitals and a doubly occupied d_{xz} orbital. Hence, Fe1 can coarsely be assigned an HS Fe³⁺ (d⁵) state and Fe2 an HS Fe²⁺ (d⁶) state. However, the calculated and experimentally observed magnetic moments are smaller than the expected ideal spin-only values of 5 and 4μ_B, respectively. Because of covalence effects, significant moments are

induced at the neighboring oxygen sites (∼0.08−0.12μ_B), which may be one of the reasons for the lower-than-expected magnetic moments at the Fe sites. In YBFO5, an Fe atom at a given site has crystallographically equivalent Fe atoms (i.e., Fe atoms with the same charge) as nearest neighbors, forming chains running along the b axis (see Figure 1b). This arrangement is less favorable with respect to structural stability than that of the YBMO5 type, and hence, such a configuration must be supported by "extra stabilization" from OO and/or SO (see below).

The orbital-projected DOSs (Figure 9a) for YBFO5 show that Fe1 has a negligible DOS in the vicinity of E_F (from −1 to 0 eV) whereas some DOS features are seen in the same energy range for Fe2. Hence, we calculated the d-orbital density matrices for Fe1 and Fe2 over an extended energy range (from −2 to 0 eV) in order to obtain a consistent picture. The $d_{x^2-y^2}$ orbital of Fe1 and the d_{xz} orbital of Fe2 form the OO pattern in YBFO5 (Figure 8b). As a result of the ordering of the $d_{x^2-y^2}$ orbital on Fe1, the Fe1−Ob bond lengths are fairly equal along the a and b directions (see Figure 1b). On the other hand, the double occupancy of the d_{xz} orbital of Fe2 lifts the degeneracy of the e_g level and leads to second-order JTD. Therefore, the square pyramids around Fe2 are somewhat distorted, with two of the four Fe2−Ob bonds elongated and two shortened within the pyramid-base plane. This finding is consistent with the results of the experimental structural study and extended-Hückel tight-binding calculations for YBFO5.[2]

Moreover, the Fe1−Ob−Fe1 AF superexchange interaction is favored because of hybridization of the $d_{x^2-y^2}$ orbital of Fe1 and the p_x and p_y orbitals of O along the b direction, and consequently, the magnetic moment at the Fe1 site is aligned along the b direction. As Fe1 has a comparatively larger moment than Fe2, it causes the magnetic moment of Fe2 to also be aligned along the b direction. Moreover, it

(35) Ravindran, P.; Fjellvåg, H.; Kjekshus, A.; Delin, A.; Eriksson, O. *Phys. Rev. B* **2002**, *65*, 064445.
(36) Vidya, R.; Ravindran, P.; Fjellvåg, H.; Kjekshus, A. *Phys. Rev. B* **2006**, *74*, 054422.

can be seen from Figure 9a that the $d_{x^2-y^2}$ orbital of Fe1 lies close to -2 eV whereas the higher-lying $d_{x^2-y^2}$ and d_{xz} orbitals of Fe2 appear in the energy range -1 to 0 eV. The hybridization interaction between these orbitals via intervening oxygen orbitals is small compared to that between the $d_{x^2-y^2}$ orbitals of neighboring Fe1 atoms. This complies with the finding that an Fe1 (Fe^{3+}) atom has another Fe1 atom instead of an Fe2 atom as its nearest neighbor along b. The same argument can be applied to Fe2 as well. Therefore Fe1 and Fe2 are arranged in chains running along the b direction, resulting in stripe-type CO as opposed to the checkerboard-type CO in YBMO5. As the Fe^{3+}–O–Fe^{3+} and Fe^{2+}–O–Fe^{2+} configurations would be electrostatically unstable, these chains are further stabilized by the AF spin arrangement between nearest-neighbor Fe atoms along the b direction. A closer inspection of the orbital-projected DOSs in Figure 9a reveals that the $d_{x^2-y^2}$ orbitals of Fe1 and Fe2 are oppositely oriented in the energy range -2 to 0 eV, leading to an AF arrangement of the Fe1 and Fe2 spins along the a direction also. Therefore, a Wollan–Koehler-type G-AF ordering occurs in YBFO5 rather than the simple G-AF-type magnetic ordering found for YBMO5 (see Figure 1a,b).

3. YBaCo$_2$O$_5$. The magnetization curve for YBCO5 showed an anomaly at 220 K that was attributed to the onset of unidirectional CO.[3] It may be worthwhile to note that the same type of ordering at virtually the same temperature was also found in HoBaCo$_2$O$_5$ and NdBaCo$_2$O$_5$, lending support to the inference that these SO and CO schemes are governed by the arrangement in the cobalt–oxygen planes.[6] The orbital-projected DOSs for the Co d states in Figure 9b show that three of the five d orbitals are singly occupied and two are doubly occupied on Co1. On the other hand, only one of the d orbitals of Co2 is doubly occupied while the remaining four are singly occupied. Therefore, Co1 and Co2 can formally be assigned as HS Co^{2+} and HS Co^{3+}, respectively, in agreement with our BEC deductions as well as previous calculations.[18] However, the calculated magnetic moments of Co1 and Co2 are smaller than the ideal spin-only values of 3 and 4μ_B, respectively, which can be attributed to covalence effects. Since the complete filling of one of the lowest-lying e_g levels on Co2 (d_{yz} in this case) lifts the degeneracy, second-order JTD occurs. This can be seen from the elongation and shortening of the Co2–Ob bonds along the pyramid-base plane (see Figure 1c). However, the non-Jahn–Teller-active Co1 (Co^{2+}) atom seems to exhibit a more-distorted square-pyramidal environment than Co2. This can be reasoned as follows.

The $d_{x^2-y^2}$, d_{xz}, and d_{yz} orbitals on Co1 appear in the energy range -1 to 0 eV, and accordingly, these orbitals are ordered on Co1 as shown in Figure 8c. On the other hand, the d_{yz} orbital on Co2 has prominent states close to E_F, whereas fewer d_{xz} states occur in the same energy range. Hence, these two orbitals enforce OO on the Co2 sites. As a result of the ordering of $d_{x^2-y^2}$ on Co1, the Co1–Ob bond is elongated along the a direction, as in the case of Mn2 in YBMO5. However, the additional ordering of the d_{xz} and d_{yz} orbitals shortens the Co1–Ob bonds along the b direction. Therefore

the square pyramids around Co1 (Co^{2+}) are more distorted than those around Co2 (Co^{3+}). This type of OO is also one of the reasons allowing two Co1 atoms to be nearest neighbors along b and two Co2 atoms similarly to become nearest neighbors. Thus, stripe-type CO results, as in the case of YBFO5. In fact, an unrestricted Hartree–Fock calculation for YBCO5[37] has shown that the stripe-type CO state becomes more stable than the checkerboard-type state as the lattice distortion increases, indicating that OO is the main reason for stabilization of stripe-type CO, consistent with our findings.

In order to improve the stability of this arrangement, two nearest-neighbor Co1 (Co^{2+}) moments are antiferromagnetically aligned along the b direction, and similarly, the two nearest-neighbor Co2 (Co^{3+}) moments are antiferromagnetically aligned. A careful look at the orbital-projected DOSs (Figure 9b) shows that the majority-spin states of the d_{xz} and d_{yz} orbitals on Co1 and the minority-spin states of these orbitals on Co2 are prominently present near E_F, enabling an AF arrangement along the a direction also. Therefore, a Wollan–Koehler-type G-AF ordering results in YBCO5, as in the case of YBFO5.

The stacking of the d_{z^2} orbitals on the Mn atoms makes the CO in YBMO5 the strongest among the studied compounds (T_{CO} is above room temperature for the Mn phase). The ordering of d_{xz} on Fe2 (Fe^{2+}) in YBFO5 is relatively easier to achieve than the complex ordering that emerges from a combination of the d_{xz} and d_{yz} orbitals on Co1 (Co^{2+}) in YBCO5. Therefore, the CO in YBFO5 is stronger than that in YBCO5, in accordance with the higher value of T_V for YBFO5 ($\sim$308 K) than for YBCO5 ($\sim$240 K).

V. Conclusions

This contribution reports on full-potential linearized augmented-plane-wave calculations for YBaMn$_2$O$_5$, YBaFe$_2$O$_5$, and YBaCo$_2$O$_5$ in paramagnetic, ferromagnetic, and antiferromagnetic configurations. The experimentally established ferrimagnetic ground state for YBaMn$_2$O$_5$ and the antiferromagnetic ground states for YBaFe$_2$O$_5$ and YBaCo$_2$O$_5$ were confirmed using GGA calculations including spin–orbit coupling. The semiconducting ground state was correctly obtained for YBaMn$_2$O$_5$ using the simple GGA+SOC calculations, whereas only the GGA+U method was able to provide semiconducting behavior for the Fe and Co variants.

An attempt to analyze the charge-ordering phenomena was made with the help of DOS plots and the Bader "atom-in-molecule" concept. Even though different amounts of charge were calculated for the Bader regions corresponding to the transition-metal atoms, these calculations were not able to reveal quantitatively correct values for the actual charge states of these atoms. However, the Born effective-charge analysis gave a good assessment of the charge states for the constituents in the YBaT$_2$O$_5$ compounds. Accordingly, the T atoms in YBaT$_2$O$_5$ can be assigned formal 3+ and 2+ charge states, and orbital-projected densities of states showed

(37) Wang, J.; Zhang, W.; Xing, D. Y. *Phys. Rev. B* **2002**, *66*, 052410.

that these are high-spin states. By comparing the orbital-ordering patterns obtained from simple rigid-band filling with those obtained from the actual calculations, we found that the simple rigid-band-filling concept is unable to account for the orbital ordering of these phases.

It can be concluded that the filling of the d orbitals (and subsequent orbital ordering) of the transition-metal atoms determines the spin and charge ordering in the $YBaT_2O_5$ phases. Even though the rigid-band approximation gave some hints about the different orbital ordering patterns to be expected, the picture deduced on this basis was absolutely nowhere near reality. In order to understand the actual situation, extensive calculations were needed, as shown here.

Moreover, visualization of ordered orbitals having the correct degree of filling and orientation enabled us to explain almost all of the structural and magnetic properties of these materials. Hence, we believe that this method of using energy-projected d-orbital density matrices can also be applied to understanding the properties of other compounds.